Effects of surfaces and macromolecular crowding on bimolecular reaction rates

Steven S. Andrews

Department of Physics, Seattle University, Seattle, WA
Division of Basic Sciences, Fred Hutchinson Cancer Research Center, Seattle, WA

E-mail: steven.s.andrews@gmail.com

Submitted to Physical Biology November 2019

Abstract. Biological cells are complex environments that are densely packed with macromolecules and subdivided by membranes, both of which affect the rates of chemical reactions. It is well known that crowding reduces the volume available to reactants, which increases reaction rates, and also inhibits reactant diffusion, which decreases reaction rates. This work investigates these effects quantitatively using analytical theory and particle-based simulations. A reaction rate equation based on these two processes turned out to be inconsistent with simulation results. However, also accounting for diffusion inhibition by the surfaces of nearby obstacles led to perfect agreement for reactions near impermeable planar membranes and improved agreement for reactions in crowded spaces. These results help elucidate reaction dynamics in confined spaces and improve prediction of in vivo reaction rates from in vitro ones.

1. Introduction

Actively growing cells have been shown to be about 17 to 26 percent protein by weight [1], with the implication that a similar fraction of a cell's volume is occupied by protein. Additional volume is occupied by nucleic acids, ribosomes, and complex sugars. Together, these result in a very crowded intracellular environment that may be more physically similar to a protein crystal or a gel than to the dilute laboratory solutions that are typically used for in vitro experiments [1].

This macromolecular crowding affects intracellular dynamics in several ways (see reviews [2, 3, 4, 5, 6]). It slows diffusion by about a factor of 5 to 10 [7, 8], it increases association reaction rate constants by an order of magnitude or more [9], it favors folded protein conformations over unfolded ones [5], and it enhances the activity of chaperones [3, 10]. Most theoretical explorations of these effects have focused on thermodynamic considerations, including particularly the reduced translational and configurational entropies of molecules that are in crowded systems [11, 12]. This entropy reduction tends to decrease the entropic benefits of dissociated states and unfolded proteins, which then shits equilibria toward associated states and folded proteins.

The effects of crowding can also be interpreted with a kinetic viewpoint. For bimolecular reactions, the reduction of available volume confines the reactants into less space, so they collide with each other more often than they would otherwise, which increases reaction rates. Vice versa, crowding also inhibits molecular motion, which decreases the rate at which reactants collide with each other and thus decreases reaction rates. Minton described these opposing effects of crowding on bimolecular reaction rates in 1990, predicting that volume reduction would be more important at low crowding densities and diffusion reduction at high crowding densities [13]. These predictions are qualitatively supported by recent experiments [9, 14, 15, 16, 17, 18, 19, 20] and modeling [21, 22, 23, 24], but a quantitative theory of reaction rates in crowded environments has not been reported previously.

This work presents a quantitative theory for the combined effects of volume reduction and diffusion inhibition on bimolecular reaction rates. It focuses on how the steady-state reaction rate constants of irreversible reactions vary with the density and sizes of inert immobile crowders. It also investigates how nearby inert planar surfaces affect bimolecular reaction rates. These analytical theories are compared against off-lattice simulations performed with the Smoldyn software, which has been thoroughly validated in prior work [25, 26, 27].

2. Theory

2.1. Reaction rates without crowders

This work builds on ideas introduced by Smoluchowski [28] and refined by Collins and Kimball [29]. For the generic irreversible reaction A + B → P, not including crowders, they showed that the rates of diffusion-influenced reactions can be computed using the radial distribution function of B molecules about A molecules, given here as $g_B(r,t)$. Doing so effectively defines a reference frame in which an A molecule is permanently at the origin and surrounded by B molecules that diffuse, in this reference frame, with the sum of the diffusion coefficients for the separate A and B molecules, D_A and D_B; this sum is called the mutual diffusion coefficient and denoted D [30]. The A and B reactants contact each other when their centers are separated by the "contact radius", σ_{AB}, which equals the sum of the reactants' physical radii, σ_A and σ_B (all molecules are assumed here to be spherical and rotationally isotropic, to diffuse ideally, and to only interact upon contact; see Figure 1A). For simplicity, it is sometimes helpful to assign the contact radius entirely to the A molecule, effectively making it a sphere of radius σ_{AB} and the B molecules into points (Figure 1B).

The radial distribution function is normalized to approach 1 at large radii and evolves according to the radially symmetric diffusion equation [31],

$$\frac{\partial g_B(r,t)}{\partial t} = -\frac{D}{r^2}\frac{\partial}{\partial r}\left[r^2\frac{\partial g_B(r,t)}{\partial r}\right]. \tag{1}$$

It also has an inner Dirichlet boundary condition, $g_B(\sigma_{AB},t) = 0$, if reaction occurs

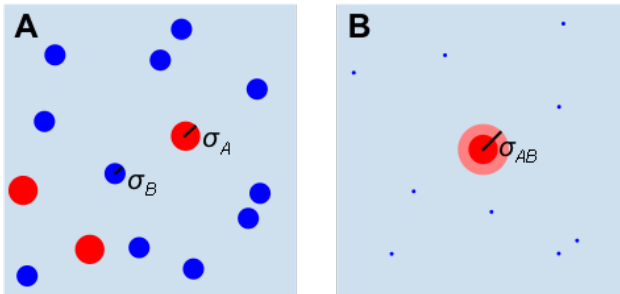

Figure 1. (A) A reactive system with A molecules in red and B molecules in blue, with respective radii σ_A and σ_B. (B) A simplified version of the same system, now with an A molecule at the origin acting as a sink that has radius σ_{AB} and B molecules reduced to points.

immediately upon contact as in the Smoluchowski model [28], or an inner Robin boundary condition,

$$\left.\frac{\partial g_B(r,t)}{\partial r}\right|_{r=\sigma_{AB}^+} = \frac{g_B(\sigma_{AB},t)}{\gamma}, \tag{2}$$

if contacting molecules have finite reactivity, as in the Collins and Kimball model [29]. This finite reactivity can arise from a reaction activation energy or can represent orientational specificity for the reactants. It is often called the intrinsic reaction rate constant [30, 32], defined as $k_{int} = 4\pi\sigma_{AB}^2 D/\gamma$.

The total reaction rate constant is the net influx of B molecules toward A molecules measured at the contact radius,

$$k(t) = 4\pi\sigma_{AB}^2 D \left.\frac{\partial g_B(r,t)}{\partial r}\right|_{r=\sigma_{AB}}. \tag{3}$$

Solving eq. 1 for the steady-state radial distribution function, $g_B(r)$, and then using it to compute the reaction rate constant with eq. 3 leads to the well-known Collins and Kimball reaction rate equation [29, 33],

$$\frac{1}{k} = \frac{1}{4\pi D\sigma_{AB}} + \frac{1}{k_{int}}. \tag{4}$$

The first term represents the time that reactants take to initially find each other through diffusion and the second is the additional time that they then take to react. Reactions are said to be diffusion-limited if the first term dominates and activation-limited if the second term dominates. Alternatively, the degree to which a reaction is diffusion-limited can be quantified with the "diffusion-limited fraction", χ, defined as

$$\chi = \frac{k}{4\pi D\sigma_{AB}}. \tag{5}$$

This value is 0 in the activation-limited extreme and 1 in the diffusion-limited extreme, and relates to γ as $\chi = \sigma_{AB}/(\sigma_{AB} + \gamma)$.

2.2. Crowder volume exclusion and diffusion reduction

Now considering crowders, suppose they have number density ρ_C, they are spherical, they are all the same size with radius σ_C, and they cannot overlap each other (Figure 2A). Combining the volume of each crowder with the crowder density shows that the fraction of the system volume that they occupy is

$$\phi = \frac{4}{3}\pi\sigma_C^3\rho_C. \tag{6}$$

However, not all of the remaining volume is accessible to the centers of the reactant molecules because the reactants have finite radii that keep their centers away from the crowder edges [34] (Figure 2B). Focusing on the B molecules (the A molecules are identical, but we choose B molecules for concreteness), define the fraction of the total system volume that is excluded to the B molecule centers as $\phi_x(\phi, \tilde{\sigma}_B)$. The tilde symbol implies a reduced radius in which the radius is divided by the crowder radius, so $\tilde{\sigma}_B = \sigma_B/\sigma_C$. Clearly, $\phi_x(\phi, \tilde{\sigma}_B) \geq \phi$ with equality only for molecules that are point particles. Figure 2C shows the relationship between $\phi_x(\phi, \tilde{\sigma}_B)$ and ϕ with different curves representing different $\tilde{\sigma}_B$ ratios. The points in the figure represent simulation data generated with the SmolCrowd software [26], which creates systems of randomly positioned spherical crowders that have non-overlapping core regions and overlapping outer regions, and then quantifies the excluded volume (see Methods). The curves in the figure were fit to the simulation data using an empirical function form, giving the relationship

$$\phi_x(\phi, \tilde{\sigma}_B) \approx 1 - \exp\left[-\phi(\tilde{\sigma}_B + 1)^3 - \phi^2\left(16.4\tilde{\sigma}_B^2 + 5.31\tilde{\sigma}_B + 0.474\right)\right]. \tag{7}$$

This fit is within 4% of all simulated values, which extend over all biologically important crowding fractions and all that are considered in this work, and can be shown to approach exactness in the limits of small ϕ and/or large $\tilde{\sigma}_B$.

The law of mass action states that reaction rates are directly proportional to each of the reactant concentrations [35], obeying the equation

$$\frac{d[\mathrm{A}]}{dt} = -k[\mathrm{A}][\mathrm{B}], \tag{8}$$

where brackets indicate concentrations. Assume that this applies within the portion of the system to which the A and B molecules are confined by the crowders; take this for now as the fraction $1-\phi_x(\phi)$ of the system volume. The observed reaction rate is always measured with respect to the total system volume rather than the accessible volume, so the concentrations in eq. 8 need to corrected to account for the different volumes. Doing so introduces a factor of $[1 - \phi_x(\phi)]^{-1}$ on the right hand side of the equation, which implies that the crowders increase the observed reaction rate constant by this factor; this is the reaction rate increase for Minton's theory [13]. A similar analysis applies if the A and B molecules have different radii. Assuming that the B molecules have smaller radii, so that their accessible region of the system volume is a superset of that which is accessible to the A molecules, then correcting eq. 8 for these volume differences shows that crowding increases the reaction rate by a factor of $[1-\phi_x(\phi, \tilde{\sigma}_B)]^{-1}$. In other

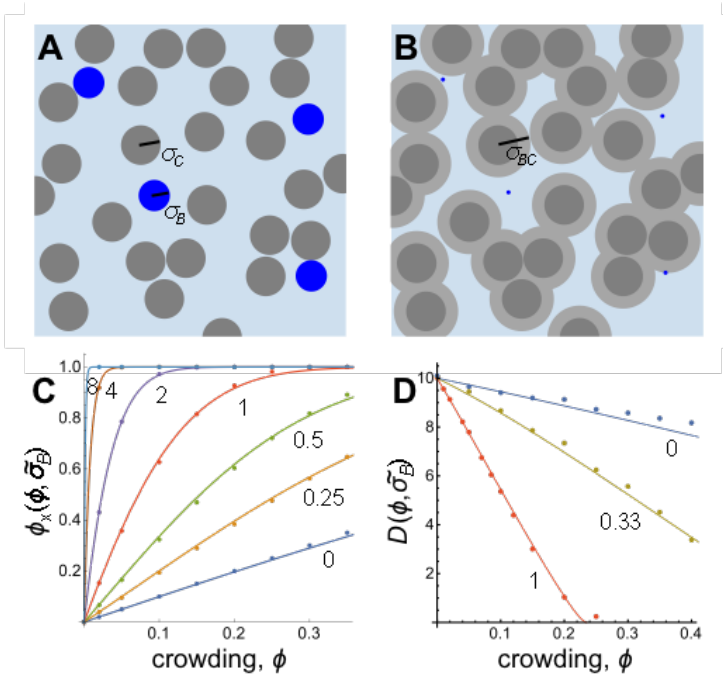

Figure 2. (A) Diagram of a crowded system, shown with B molecules and gray crowders with respective radii σ_B and σ_C; crowders occupy volume fraction ϕ. (B) An equivalent system showing the B molecule centers and the total volume excluded by the crowders, now with effective radii $\sigma_{BC} = \sigma_B + \sigma_C$; they exclude volume fraction $\phi_x(\phi, \tilde{\sigma}_B)$. (C) Relationship between occupied and excluded volume fractions for the $\tilde{\sigma}_B$ values shown. (D) Diffusion coefficients for B molecules with the $\tilde{\sigma}_B$ values shown, with $D_0 = 10$ µm^2/s.

words, the effective volume for the reaction is the available volume for the less confined reactant. For convenience, we define $\phi_x(\phi)$ as the excluded volume for the less confined of either the A or B molecules.

The crowders also reduce diffusion coefficients because they physically block many diffusive trajectories (Figure 2D). Points in this figure were computed by simulating diffusion of tracers, which had the same radii as B molecules but did not participate in reactions, among immobile spherical crowders using the Smoldyn software. Diffusion coefficients were calculated from final mean square displacement values (see Methods). The lines in the figure were not fit to the data but represent the function

$$D(\phi, \tilde{\sigma}_B) = D_0 \frac{[1 - \phi_x(\phi, \tilde{\sigma}_B)/0.955]^{1.47}}{1 - \phi_x(\phi, \tilde{\sigma}_B)}, \tag{9}$$

where D_0 is the diffusion coefficient in the absence of crowders [36]. This function fit well to tracer diffusion in systems that were similar to the ones investigated here [36] and also agrees well with the data generated here. Although not explored in this work, note that diffusion coefficients are substantially larger if the crowders are mobile [37].

Combining the effects for the reduced available volume and slowed diffusion

coefficients modifies the Collins and Kimball reaction rate equation from eq. 4 to

$$\frac{1}{k(\phi)} = [1 - \phi_x(\phi)] \left[\frac{1}{4\pi D(\phi)\sigma_{AB}} + \frac{1}{k_{int}} \right], \tag{10}$$

where $D(\phi)$ is the mutual diffusion coefficient in the crowded environment, which is equal to $D(\phi, \tilde{\sigma}_A) + D(\phi, \tilde{\sigma}_B)$. Figure 3 compares this prediction with simulation data for diffusion-limited and nearly activation-limited reactions in crowded systems. The prediction and the simulation results disagree strongly, showing that these two effects are inadequate for quantitatively explaining how crowding affects reaction rates. As shown below, an important effect that was ignored here is inhibition of diffusion by nearby crowder surfaces.

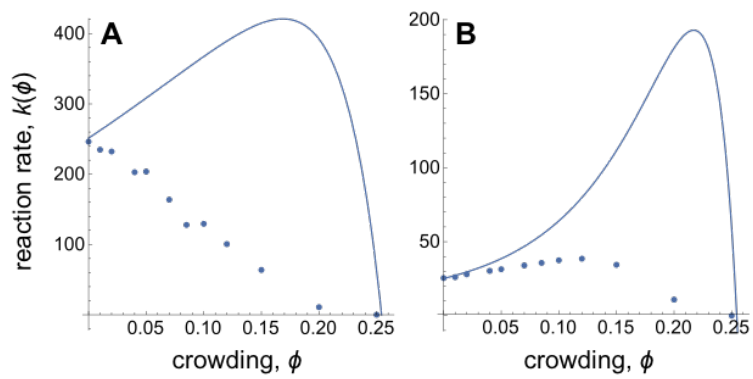

Figure 3. Effective reaction rate constants for (A) diffusion-limited and (B) nearly activation-limited reactions. Points are from Smoldyn simulations and lines from eq. 10. Parameters: $\sigma_A = \sigma_B = \sigma_C = 0.5$ nm, $D_A = D_B = 10$ μm^2/s, $\chi = 1$ in panel A and 0.1 in panel B.

2.3. Surface effect of a planar surface

To illustrate the effect of nearby surfaces, consider a system in which we again consider the reaction A + B → P but with a simpler system geometry. Now, a single A molecule sink is fixed at distance x_A from an impermeable planar surface that is located at $x = 0$, and B molecules diffuse and get absorbed by the sink (Figure 4A). We wish to solve for the steady-state reaction rate constant while accounting for the surface's influence.

As usual, it's convenient to focus on the centers of the B molecules rather than their edges, which effectively moves the surface location to σ_B and increases the A molecule radius to σ_{AB} (Figure 4B). Define $C_B(\mathbf{x}, t)$ as the mean B molecule concentration at position $\mathbf{x}$ and time t. This function approaches the overall B molecule concentration at large distances from the A molecule but is smaller at closer distances due to absorption. The system has a Neumann boundary condition at the effective planar surface,

$$\left. \frac{\partial C(\mathbf{x}, t)}{\partial x} \right|_{x=\sigma_B} = 0, \tag{11}$$

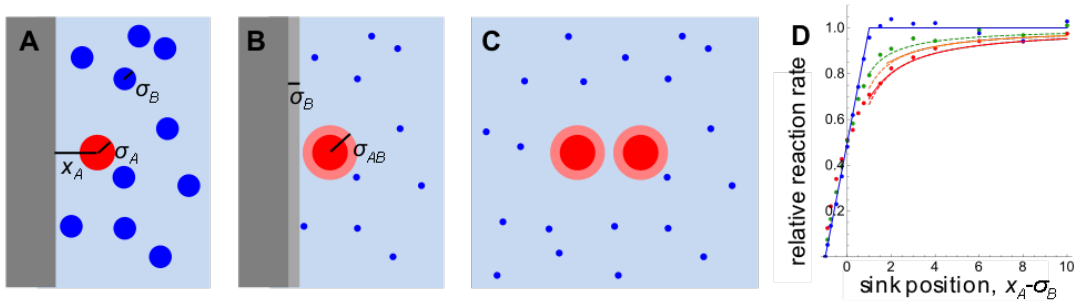

Figure 4. (A) A sink, in red, near an impermeable surface, in gray. B molecules, in blue, get absorbed by the sink. (B) A simplified version of the same system, with the B molecule radii effectively added to the surface and sink. (C) A further simplification using the method of images. (D) Relative reaction rate as a function of distance from the surface. Red represents diffusion-limited, orange is for $\chi = 0.7$, green is for $\chi = 0.5$, and blue is for activation-limited. Points are from Smoldyn simulations, solid lines from theory, and dashed lines from eq. 13.

to represent the fact that there cannot be concentration gradients perpendicular to impermeable surfaces. As before, the sink has a Robin boundary condition at the contact radius, σ_{AB}, to represent reactions (eq. 2). The Neumann boundary condition at the planar surface is easiest to address with the method of images [38]. Here, this means that a mirror image of the real system, including the A molecule sink, is introduced on the unphysical side of the surface. By symmetry, this modified system automatically obeys the Neumann boundary condition at $x = \sigma_B$, allowing the presence of the surface to be neglected (Figure 4C).

The steady-state reaction rates have been solved exactly for this symmetric system, both for the case where reactants react immediately upon contact [39] as in the Smoluchowski model, and where they have finite reactivity [40] as in the Collins and Kimball model, provided that the sink doesn't touch the planar surface. The former result is [39]

$$\frac{k(x_A)}{k_0} = 1 - \sum_{m=2}^{\infty} (-1)^m \frac{\sinh \mu_0}{\sinh m\mu_0} \tag{12}$$

where k_0 is the reaction rate constant without the surface and the μ_0 parameter is determined from $\cosh \mu_0 = (x_A - \sigma_B)/\sigma_{AB}$. The latter result, for the Collins and Kimball model, is not repeated here because it is complicated, but is described in ref. [40]. Figure 4D shows these analytic solutions with red and orange solid lines. Both solutions are closely approximated by

$$\frac{k(x_A)}{k_0} = \left[1 + \frac{\chi \sigma_{AB}}{2(x_A - \sigma_B)}\right]^{-1}. \tag{13}$$

This equation, which I derived using a particle emission model as described below, extends a result for the Dirichlet boundary condition that is given in [39]. Figure 4D shows these approximate solutions with dashed lines. Both the exact and approximate solutions agree well with simulation results, shown in the figure with points.

Reaction rates can also be solved when the sink overlaps the planar surface for a few special cases. One arises when the center of the A molecule is exactly at the effective surface, $x_A = \sigma_B$. Here, the actual A molecule sink exactly overlaps its image to make a single sphere, so the reaction rate per sink is half of that for a single isolated sink. This gives $k(\sigma_B)/k_0 = 1/2$, regardless of whether the reaction is diffusion-limited, activation-limited, or in between. Another solution arises when the sink is fully behind the surface, where it's inaccessible and hence must have zero reaction rate. This implies that $k(x_A) = 0$ for $x_A \leq -\sigma_A$ or, equivalently, for $x_A - \sigma_B \leq -\sigma_{AB}$. Finally, in the activation-limited extreme, absorption at the sink depends only on the amount of exposed sink surface area, so $k(x_A)/k_0 = 1$ for $x_A - \sigma_B \geq \sigma_{AB}$ and $k(x_A)/k_0 = (x_A - \sigma_B + \sigma_{AB})/2\sigma_{AB}$ for $-\sigma_{AB} \leq x_A - \sigma_B \leq \sigma_{AB}$. Figure 4D shows this last solution with a blue line.

This analysis shows that the mere presence of an impermeable surface can substantially decrease the reaction rate constant for nearby molecules. This reduced reactivity arises from the fact that the surface inhibits diffusion in its vicinity, albeit only at the surface and perpendicular to it, which then reduces the net diffusive flux of reactants toward each other. As another view of the same phenomenon, each A molecule is effectively competing with its mirror image for B molecules, thus causing it to absorb fewer B molecules than it would when far from a surface.

The finding that reaction rates are slower near surfaces raises the intriguing possibility that cells might control some reaction rates by regulating the precise locations of reactive sites that are near membranes. For example, cells could extend or retract specific membane-bound receptors by small amounts to modulate their rates of ligand binding. I am not aware of examples where there is evidence of this but the necessary protein conformational changes are well within the realm of typical biochemical behaviors.

2.4. Surface effect of spheres

Given that proximity to a planar surface slows reaction rates, it makes sense that proximity to the multiple spherical surfaces that arise in crowded systems would also slow reaction rates. This is an aspect of diffusion inhibition by crowders but is independent of the inhibition considered previously in eq. 10. To address this, we would like to solve for the influx rate of a sink that is surrounded by randomly placed impermeable spheres.

Unfortunately, the solutions for reaction rates near planar surfaces (eq. 12) do not generalize to spherical surfaces. However, an approximate solution can be found by inverting the problem to consider emission of B molecules out of a point source instead of absorption of B molecules into a sink. This inverted problem obeys the same diffusion equation and has the same Neumann boundary conditions at the crowder surfaces but is reversed so that there is net outward flow instead of net inward flow, and the concentration approaches zero instead of a finite value at infinity. The only substantial change is that the Robin boundary condition at the contact radius (eq. 2)

is ignored for now.

Consider an emitter that is at the origin and emits B molecules at unit rate, and a single spherical crowder of radius σ_C that is placed with its center at distance r_0 from the origin (Figure 5A). As usual, it is easiest to focus on the centers of the B molecules, giving the crowder an effective radius of $\sigma_{BC} = \sigma_B + \sigma_C$. Dassios and Sten showed that the Neumann boundary condition at the effective crowder surface can, again, be addressed with the method of images [41]. In this case, there is a "point image emitter" that is within the crowder and at distance $r' = r_0 - \sigma_{BC}^2/r_0$ from the origin, which emits at rate $q_{pt.} = \sigma_{BC}/r_0$, and also a "line image emitter" that extends from r' to r_0 and emits at a continuous rate over its entire length with emission density $q_{line} = -1/\sigma_{BC}$. The line emitter emits at a negative rate, which is mathematically sensible as stated, or can be considered physically as emission of anti-particles that anhiliate with normal particles upon collision. Figure 5B shows that including these image emitters creates a zero concentration gradient at the effective crowder surface, as desired. Note that total emission from the point and line image emitters adds to zero, meaning that these image emitters are neither net sinks nor net sources.

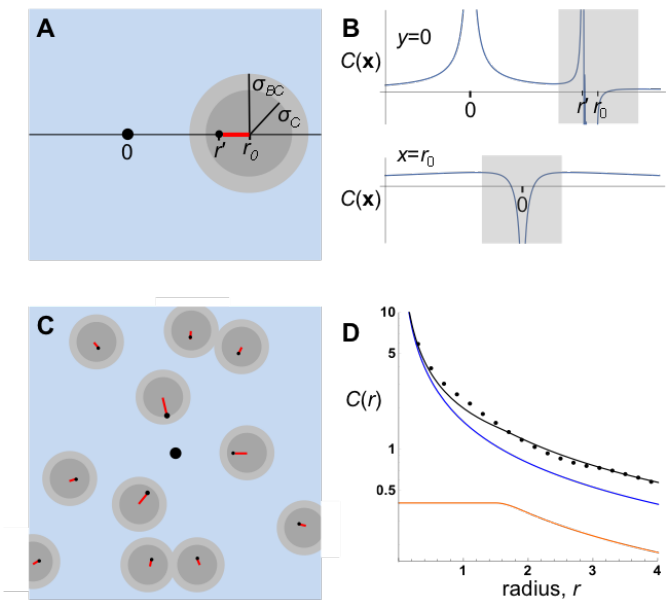

Figure 5. (A) An emitter at the origin, shown at $x = 0$ in black, and its image emitters within a spherical crowder, shown as a black dot at $x = r'$ for the point emitter and as a red line for the line emitter. (B) The total emitted B molecule concentration measured along the x-axis at top and along y at $x = r_0$ on the bottom. Dark bands represent the crowder, at the edges of which the Neumann boundary condition is observed. (C) An emitter at the origin surrounded by randomly positioned crowders, each of which has point and line emitters. (D) B molecule concentration as a function of radius for the system shown in panel C. The blue line represents the concentration from just the central emitter, orange represents the concentration from the image emitters, and black represents the total concentration. Dots represent data from a Smoldyn simulation using impermeable spheres rather than image emitters.

We extend this image emitter solution to many crowders (Figure 5C) using a mean field approximation, replacing discrete point and line image emitters for individual crowders with a density of point and line image emitters that arises from the density of crowders. In the process, we only consider images that arise from the B molecule emitter at the origin, while ignoring higher order images of images. Normalized to an overall crowder density of $\rho_C = 1$, the density of emission at radius r' from the origin that arises from point image emitters is

$$q_{pt.}(r') = \frac{4\pi r_0^2 dr_0 g_C(r_0)}{4\pi r'^2 dr'} \frac{\sigma_{BC}}{r_0} = \frac{\sigma_{BC} g_C(r_0)}{r'^2} \frac{dr_0}{dr'} \tag{14}$$

where $g_C(r_0)$ is the radial distribution function of crowders about the origin. In the first equality, the numerator of the first term gives the number of crowders that have their centers between r_0 and r_0+dr_0, the second term is the emission rate from these crowders, and the denominator of the first term converts the result back to a density at radius r'. The r_0 values in this emission density can be replaced using $r_0 = (r' + \sqrt{r'^2 + 4\sigma_{BC}^2})/2$, from the relationship between r_0 and r' given above, but this only complicates the result. The density of emission at radius r' from line image emitters requires integration over all of the crowders that contribute to line image emission at this location, leading to

$$\begin{aligned} q_{line}(r') &= \frac{1}{4\pi r'^2} \int_{r'}^{r_0} 4\pi r''^2 g_C(r'') \frac{-1}{\sigma_{BC}} dr'' \\ &= -\frac{1}{\sigma_{BC} r'^2} \int_{r'}^{r_0} r''^2 g_C(r'') dr''. \end{aligned} \tag{15}$$

The total density of emission at r', still normalized to unit crowder density, is the sum of these contributions,

$$q(r') = q_{pt.}(r') + q_{line}(r'). \tag{16}$$

This image emitter density depends only on the crowder locations and effective sizes, so it can be evalulated from only knowledge of $g_C(r_0)$ and σ_{BC}, meaning that details about A molecules, reactions, and all concentrations are unimportant here.

Next, we compute the steady-state density of emitted B molecules from both the emitter at the origin and all of the image emitters. We do so with a Green's function approach, using the fact that the steady-state density of emitted particles from a thin spherical shell of emitters that is located at radius r_s from the origin is [31]

$$C(r) = \frac{1}{4\pi D} \left\{ \begin{array}{ll} r_s^{-1} & r < r_s \\ r^{-1} & r \geq r_s \end{array} \right\}. \tag{17}$$

Integrating this kernel over the actual density of emitters, including the emitter at the origin and all of the image emitters (eq. 16), gives the average concentration of emitted molecules as a function of radius as

$$C(r) = \frac{1}{4\pi D r} + \frac{\rho_C}{D} \left[\frac{1}{r} \int_0^r r'^2 q(r') dr' + \int_r^\infty r' q(r') dr' \right]. \tag{18}$$

Figure 5D shows the emitted particle density for the case where $\sigma_{BC} = 1$ and $g_C(r_0)$ is a step function that is 0 for $r_0 < 2$ and 1 for $r_0 > 2$. The blue line represents the first term of eq. 18 (from the emitter at the origin), the orange line represents the second term (from the image emitters), and the black line represents their sum. Points in the figure show that simulation results, which were computed with randomly placed impermeable spheres rather than image emitters, agree well with the theory.

Some transformations convert this concentration result, eq. 18, for molecule emission back to the desired radial distribution function for a reactive sink. The sign is reversed to change from emission to absorption, the concentration is rescaled so that it obeys the desired Robin boundary at the contact radius (which can now be obeyed due to the spherical symmetry introduced by the mean field approach), and the result is offset so that the radial distribution approaches 1 at large radii. Together these give

$$g_B(r) = 1 - \frac{C(r)}{C(\sigma_{AB}) + \gamma C'(\sigma_{AB})}, \tag{19}$$

where $C'(\sigma_{AB}) = dC(r)/dr|_{\sigma_{AB}}$. For example, if there are no crowders, then $C(r) = 1/4\pi Dr$, which transforms to the radial distribution function $g_B(r) = 1 - \sigma_{AB}^2/r(\sigma_{AB} + \gamma)$, as it should be for the Collins and Kimball model [25]. Substituting this transformation into eq. 3 gives the steady-state reaction rate constant in terms of the concentration of emitted B molecules,

$$k = -4\pi\sigma_{AB}^2 D \frac{C'(\sigma_{AB})}{C(\sigma_{AB}) + \gamma C'(\sigma_{AB})}. \tag{20}$$

If there are no image emitters within radius σ_{AB}, justified below, then this reaction rate equation can be expanded using eq. 18 and then simplified to

$$\frac{1}{k} = \frac{1}{4\pi D\sigma_{AB}} + \frac{1}{k_{int.}} + \frac{\rho_C}{D}\int_{\sigma_{AB}}^{\infty} r' q(r') dr'. \tag{21}$$

The first two terms are the same as those in the Collins and Kimball reaction rate equation, eq. 4, while the last term is new and accounts for surface effects. Define Q as a scaled version of this new term,

$$Q = \frac{1}{\sigma_{BC}^2}\int_0^{\infty} r' q(r') dr', \tag{22}$$

where the lower integration limit was reduced to 0 for simplicity but didn't change the integral's value because of the assumption of no image emitters within σ_{AB}. This is a unitless number that quantifies the magnitude of the surface effect that arises from the structure of the crowded environment.

To finish converting from the emission model to the absorption model, we note that equation 21 is based on image emitters rather than actual crowders, so it does not account for either the excluded volumes of the crowders or their effects on diffusion coefficients. We include these effects in the same way that we did for eq. 10, to give a final reaction rate equation for irreversible reactions in crowded environments,

$$\frac{1}{k(\phi)} = [1 - \phi_x(\phi)]\left[\frac{1}{4\pi D(\phi)\sigma} + \frac{1}{k_{int.}} + \frac{\rho_C Q \sigma_{BC}^2}{D(\phi)}\right]. \tag{23}$$

This is the complete equation for the theory developed here, now accounting for volume exclusion, diffusion inhibition, and crowder surface effects.

However, we still need to compute Q, which comes from the crowder radial distribution function, $g_C(r_0)$. Ignoring the structured layers that arise in densely packed hard spheres [42], the obvious first-order approximation is that $g_C(r_0)$ should be a step function that is 0 for $r_0 < \sigma_{AC}$ (where $\sigma_{AC} = \sigma_A + \sigma_C$) to account for the excluded volumes of the A molecules and crowders, and 1 for larger r_0 values. This is presumably a reasonable approximation for the actual distribution of the crowders. However, looking back to eqs. 14 and 15 shows that the crowder radial distribution function was only used for placing image emitters that would then combine with the actual emitter to produce the desired Neumann boundary conditions. If the emitter at the origin cannot emit in a particular direction due to a particular crowder being too close on that side, meaning that a B molecule cannot fit between the A molecule and crowder, then no image emitters should be included in that crowder. Likewise, in the absorption problem, if a B molecule cannot fit between an A molecule and a crowder, then that side of the A molecule cannot react with the B molecule and is not competing with its image for the B molecule. For this reason, it's more accurate to use a crowder radial distribution function that has its step at one B molecule diameter farther away from the A molecules than it would otherwise, placing the step at $\sigma_{ABBC} = \sigma_A + 2\sigma_B + \sigma_C$,

$$g_C(r_0) = \left\{ \begin{array}{ll} 0 & r_0 < \sigma_{ABBC} \\ 1 & r_0 > \sigma_{ABBC} \end{array} \right\}. \tag{24}$$

This radial distribution function justifies the assumption that there were no image emitters within σ_{AB} that was made when computing eq. 21; the closest possible crowder that is included has its center at radius σ_{ABBC} and its point image emitter is at $\sigma_{ABBC} - \sigma_{BC}^2/\sigma_{ABBC}$, which is neccessarily greater than σ_{AB}. Using this crowder radial distribution function, Q evaluates to

$$Q = -\frac{1}{6}\left[2\nu^3 \ln\left(1 - \frac{1}{\nu^2}\right) + \ln\left(\frac{\nu - 1}{\nu + 1}\right) + 2\nu\right] \tag{25}$$

where $\nu = \sigma_{ABBC}/\sigma_{BC}$. For example, if $\sigma_A = \sigma_C$, then $\nu = 2$ for all σ_B values, and $Q = 0.283$.

Red lines in Figure 6 compare the theoretical reaction rate constant from eq. 23, which accounts for surface effects, with simulation data, shown with points. Agreement is reasonably good for low to medium crowding densities over a wide range of system parameters, including different relative sizes of σ_A, σ_B, and σ_C, and different amounts of diffusion influence on reactions. Furthermore, agreement at low crowder densities could not be improved significantly by varying the Q value in eq. 23, showing that the theory agrees with the data about as well as possible to first order in ρ_C and that further improvements would require higher order terms. However, the theory substantially overestimates reaction rate constants at high crowding densities, which is discussed below. At all crowder densities, accounting for surface effects, eq. 23, improves accuracy

substantially over our initial theory that ignored them, eq. 10. Note that there are no fittable parameters in either theory.

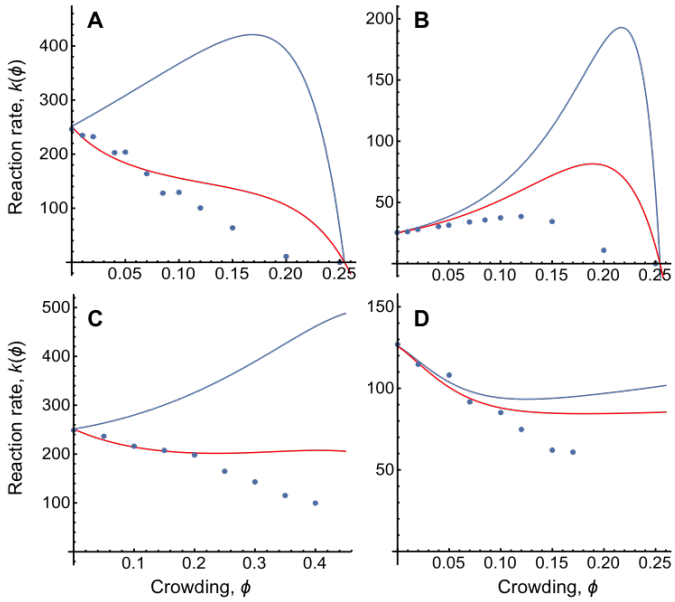

Figure 6. Reaction rates as a function of crowding for different parameter values. Points represent simulation data, blue lines represent a theory that ignores surface effects, eq. 10, and red lines represent the theory with surface effects, eq. 23. (A) Diffusion-limited reactions with all species the same size: $\chi = 1$, $\sigma_A = \sigma_B = \sigma_C = 0.5$ nm. (B) Nearly activation-limited reactions with all species the same size: $\chi = 0.1$, $\sigma_A = \sigma_B = \sigma_C = 0.5$ nm. (C) Diffusion-limited reactions with larger crowders: $\chi = 1$, $\sigma_A = \sigma_B = 0.5$ nm, $\sigma_C = 2$ nm. (D) Diffusion-influenced reactions with point-like B molecules: $\chi = 0.5$, $\sigma_A = 1$ nm, $\sigma_B = 0$ nm, $\sigma_C = 0.5$ nm. In all cases, A and B diffusion coefficients were 10 $\mu m^2/s$ and their interaction radius, σ_{AB}, was 1 nm.

3. Discussion

Minton described two opposing effects of macromolecular crowding on bimolecular reaction rates, which were that volume exclusion should accelerate reactions and diffusion inhibition should slow them. This work addressed the topic quantitatively and found that a simple interpretation of these effects, eq. 10, strongly disagreed with simulation results, substantially overestimating reaction rate constants. To investigate whether the disagreement might arise from neglect of the Neumann boundary conditions that must exist at the crowder surfaces, it then investigated the rates of reactions that take place near impermeable planar surfaces. Surface proximity was found to substantially slow reactions, eqs. 12 and 13, even when reactants were several radii away from the surface. This surface effect was then applied to the macromolecular crowding case using a mean field approximation, eventually yielding a theoretical rate equation that accounted for volume exclusion, diffusion inhibition, and also the Neumann boundary conditions at the crowder surfaces, eq. 23. This result agrees well

with simulation data for low and medium crowding densities, but still overestimates reaction rates at high densities.

Several possible reasons could explain the overestimates at high densities. (1) The mean field theory developed in eq. 16 only includes images of the central emitter, while ignoring higher order images of images. Because the first order images in each crowder have positive emission toward the origin and negative emission away from the origin, their images would add to the existing surface effect to make it stronger. This means that accounting for these effects would modify the theory in the correct direction. However, the total emission from each crowder adds to zero so it's unlikely that second or higher order images would have a large effect. Further, simulation and theory agreed well for a central emitter (Figure 5D), again suggesting that this effect is minimal. (2) The mean field theory treats every crowder as an isolated sphere of the same size, ignoring the fact that the effective radii of multiple crowders can overlap each other to create larger obstacles (Figure 2B). These larger obstacles should have greater surface effects because molecules have to diffuse a longer distance to get around them. (3) The analysis of surface effects accounts for all crowders that are farther than σ_{ABBC} distance from each A molecule center, while ignoring any crowders that are inside of that radius. Those very close crowders don't decrease reaction rates through the surface effect considered here, but would instead decrease reaction rates by reducing access between A and B molecules; this effect is ignored.

While it would be nice to compare these theoretical predictions with experiment, existing experimental data are unfortunately inadequate due to lack of breadth of parameters investigated, insufficiently characterized reaction dynamics, and/or presence of artifacts from non-specific binding or other contributions [12]. Instead, simulations are the only method currently available for producing data that can test these theories quantitatively. Furthermore, Smoldyn is essentially the only adequate simulator at present because on-lattice simulators introduce substantial artifacts [43] and other off-lattice simulators are substantially less accurate for simulations at the necessary size scale [44].

It would be straightforward to extend the theory developed here to account for crowders with a distribution of sizes rather than the single size assumed here. If they are still spherical, each crowder in the distribution could still be represented with point and line image emitters, and the effects of those emitters would still add linearly (this approach also works for non-spherical crowders but would become much more complicated). At the end, the only change would be that the single crowder number density value, ρ_C, would be replaced by a separate density for each crowder size or with a density function, $\rho_C(\sigma_C)$. Adding or integrating over these would then yield the surface effect term for eq. 23.

On the other hand, it may be more difficult to extend these results to account for mobile crowders. Preliminary investigations showed that both the starting theory, eq. 10, and the improved version that accounts for surface effects, eq. 23, overestimated reaction rates even at very low crowding densities. I speculate that this occurs because

the excluded volume correction term, $[1 - \phi_x(\phi)]^{-1}$, overestimates the excluded volume effect and thus predicts too fast reaction rates. While stationary crowders clearly remove $\phi_x(\phi)$ fraction of volume from the system, it may be that mobile crowders effectively remove less volume because their motion constantly opens up new volume, even while removing other volume.

Two primary goals of this work were to build a deep understanding of reactions in crowded spaces and to create a theory that enables one to accurately convert between reaction rates in intracellular environments and those measured in dilute solutions. The work described here does not achieve either goal in its entirety but is a significant step in the right direction. It is substantially better than previous theories, shows what types of effects are likely to be important, and identifies topics for further study.

4. Methods

Fields of randomly located crowded spheres were generated with SmolCrowd version 2 [26, 27]. These spheres had inner portions with radius σ_c that did not overlap and outer portions with radius σ_{BC} that could overlap (typically, $\sigma_C = 0.5$ nm and $\sigma_{BC} = 1$ nm). SmolCrowd's algorithm is that it adds randomly placed spheres to the system volume one at a time, rejecting trial locations that would produce inner-portion overlap with an existing sphere. After many sequential failed trials (equal to ratio of the system to sphere volumes), SmolCrowd removes a randomly chosen sphere, and then returns to trying to add more. It continues until the requested crowding fraction is achieved. It ignores the existing sphere distribution when generating trial locations and when removing spheres in order to preserve an unbiased random crowder distribution.

SmolCrowd computed the occupied volume fraction, ϕ, using eq. 6 and the excluded volume fraction, $\phi_x(\phi)$, by randomly choosing 10^5 points within the simulation volume and determining what fraction of them were within σ_{BC} of a sphere center. In simulations that had a central emitter (e.g. Figure 5D), spheres were prevented from having their inner edges within 1 nm of the origin or their outer edges beyond 10 nm from the origin. Other simulations used periodic boundary conditions, for which SmolCrowd duplicated all spheres that overlapped system boundaries as needed.

Diffusion and reaction simulations were run with Smoldyn version 2.61 [26, 45] using a cubical system that was 50 nm on each side, typically with periodic boundary conditions. All of Smoldyn's algorithms approach exactness in the limits of short time steps, so simulations were made accurate by reducing time steps until simulation results stopped changing, and also did not change with a further 5-fold reduction in time step lengths; time steps ranged from 0.0002 μs to 0.005 μs. Simulations ran until all A molecules had reacted or for 10 μs of simulated time, whichever came first. Smoldyn represented the crowders generated by SmolCrowd as immobile reflective spherical surfaces. Simulations typically started with 1000 each of A, B, and tracer molecules, each represented as simple points. Each diffused at 10 $\mu m^2/s$, which is a typical intracellular diffusion coefficient [7]. The tracers did not interact with other molecules but were

included to measure diffusion coefficients, which was done by quantifying their mean square displacements, $\langle x^2 \rangle$, and computing the diffusion coefficient from $D = \langle x^2 \rangle / 6\Delta t$ where Δt is the simulation time. Mean square displacements generally increased linearly over time, showing normal diffusion, although some anomalous subdiffusion [46, 47, 48] was observed for excluded volume fractions of 0.9 and above. The fact that diffusion was predominantly normal is consistent with the use of monodisperse crowders and simulations that ran long enough that most tracers diffused tens of times farther than the crowder radii.

Simulated reactions used the formula A+B $\rightarrow$ B, which simplified analysis by maintaining a constant B concentration. A molecules did not interact with other A molecules, or B molecules with other B molecules, including through excluded volume interactions, which simplified simulations and meant that excluded volume arose only from crowders. Reactions were interpreted using a model that I call the two-radius Smoluchowski model, in which reactants nominally interact when they are within a contact radius of each other, σ_{AB}, but don't actually react until they are at a smaller radius, σ_T, where they always react. The reaction rate constant in this model is $4\pi\sigma_T D$, which is smaller than the diffusion-limited rate constant by a factor of σ_T/σ_{AB}, so the diffusion-limited fraction value in this model is $\chi = \sigma_T/\sigma_{AB}$. This model is identical to the Collins and Kimball model for all radii that are larger than the contact radius. Because Smoldyn simulations use finite time steps, it used a slightly larger reaction radius than σ_T in order to produce the desired reaction rate constant, as described in ref. [25]. Steady-state rate constants in the crowded systems were quantified by fitting the number of A molecules in the system over time with an exponential decay function for reactions that were nearly activation-limited, or by fitting the time-dependent numerical rate constant with a function with the form $c_1(1 + c_2/\sqrt{t})$ for reactions that were nearly diffusion-limited, where c_1 and c_2 are fitting parameters and t is the time [24]; this function has the same form as the time-dependent Smoluchowski reaction rate constant [30]. In all cases, these functions fit the data closely.

5. Acknowledgements

I thank Otto Berg, Ethan Hunt, Sam Isaacson, Satya Arjunan, and Hartmut Kuthan for helpful discussions.

6. References

[1] Fulton A B 1982 *Cell* **30** 345–347
[2] Zimmerman S B and Minton A P 1993 *Annual review of biophysics and biomolecular structure* **22** 27–65
[3] Ellis R J 2001 *Trends in biochemical sciences* **26** 597–604
[4] Hall D and Minton A P 2003 *Biochimica et Biophysica Acta (BBA)-Proteins and Proteomics* **1649** 127–139
[5] Zhou H X, Rivas G and Minton A P 2008 *Annual review of biophysics* **37** 375
[6] Mourão M A, Hakim J B and Schnell S 2014 *Biophysical journal* **107** 2761–2766

[7] Dix J A and Verkman A 2008 *Annu. Rev. Biophys.* **37** 247–263
[8] Hall D and Hoshino M 2010 *Biophysical reviews* **2** 39–53
[9] Rivas G, Fernández J A and Minton A P 2001 *Proceedings of the National Academy of Sciences* **98** 3150–3155
[10] Elcock A H 2003 *Proceedings of the National Academy of Sciences* **100** 2340–2344
[11] Minton A P 1983 *Molecular and cellular biochemistry* **55** 119–140
[12] Rivas G and Minton A P 2016 *Trends in biochemical sciences* **41** 970–981
[13] Minton A P 1990 *International Journal of Biochemistry* **22** 1063–1067
[14] Rivas G, Fernandez J A and Minton A P 1999 *Biochemistry* **38** 9379–9388
[15] Hatters D M, Minton A P and Howlett G J 2002 *Journal of Biological Chemistry* **277** 7824–7830
[16] Uversky V N, M Cooper E, Bower K S, Li J and Fink A L 2002 *FEBS letters* **515** 99–103
[17] Munishkina L A, Cooper E M, Uversky V N and Fink A L 2004 *Journal of Molecular Recognition* **17** 456–464
[18] Homchaudhuri L, Sarma N and Swaminathan R 2006 *Biopolymers: Original Research on Biomolecules* **83** 477–486
[19] Moorthy J, Burgess R, Yethiraj A and Beebe D 2007 *Analytical chemistry* **79** 5322–5327
[20] Neff K L, Offord C P, Caride A J, Strehler E E, Prendergast F G and Bajzer Ž 2011 *Biophysical journal* **100** 2495–2503
[21] Sun J and Weinstein H 2007 *The Journal of chemical physics* **127** 10B617
[22] Wieczorek G and Zielenkiewicz P 2008 *Biophysical journal* **95** 5030–5036
[23] Kim J S and Yethiraj A 2009 *Biophysical journal* **96** 1333–1340
[24] Andrews S S, Arjunan S N, Balbo G, Bittig A T, Feret J, Kaizu K and Liu F 2015 Simulating macromolecular crowding with particle and lattice-based methods (Team 3) *Multiscale Spatial Computational Systems Biology* ed Gilbert D, Heiner M, Takahashi K and M U A pp 170–187
[25] Andrews S S and Bray D 2004 *Physical Biology* **1** 137
[26] Andrews S S, Addy N J, Brent R and Arkin A P 2010 *PLoS Comput. Biol.* **6** e1000705
[27] Andrews S S 2012 Spatial and stochastic cellular modeling with the Smoldyn simulator *Bacterial Molecular Networks* (Springer) pp 519–542
[28] Smoluchowski M v 1917 *Z. Phys. Chem* **92** 9
[29] Collins F C and Kimball G E 1949 *Journal of Colloid Science* **4** 425–437
[30] Rice S A 1985 *Diffusion-Limited Reactions* (Elsevier)
[31] Crank J 1975 *The Mathematics of Diffusion* 2nd ed (Clarendon Press, Oxford)
[32] Keizer J 1987 *Chemical Reviews* **87** 167–180
[33] Noyes R M 1961 *Prog. React. Kinet* **1** 129–160
[34] Minton A P 2001 *Journal of biological chemistry* **276** 10577–10580
[35] Waage P and Guldberg C M 1864 *Forhandlinger: Videnskabs-Selskabet i Christiania* 35 (translated by H.I. Abrash in *Journal of Chemical Education*, 63:1044, 1986)
[36] Novak I L, Kraikivski P and Slepchenko B M 2009 *Biophysical journal* **97** 758–767
[37] Speedy R J 1987 *Molecular Physics* **62** 509–515
[38] Jackson J D 1999 *Classical electrodynamics* (AAPT)
[39] Samson R and Deutch J 1977 *The Journal of Chemical Physics* **67** 847–847
[40] Zoia G and Strieder W 1998 *The Journal of chemical physics* **108** 3114–3118
[41] Dassios G and Sten J C E 2012 *Mathematical Methods in the Applied Sciences* **35** 482–496
[42] Chang J and Sandler S I 1994 *Molecular Physics* **81** 735–744
[43] Meinecke L and Eriksson M 2016 *IET systems biology* **11** 55–64
[44] Andrews S S 2018 *Encyclopedia of Computational Neuroscience* **10** 978–1
[45] Andrews S S 2017 *Bioinformatics* **33** 710–717
[46] Saxton M J 1994 *Biophysical journal* **66** 394–401
[47] Banks D S and Fradin C 2005 *Biophysical journal* **89** 2960–2971
[48] Marquez-Lago T, Leier A and Burrage K 2012 *Systems Biology, IET* **6** 134–142